Available online at www.sciencedirect.com
SCIENCE DIRECT®
Computational Materials Science 32 (2005) 370–377
COMPUTATIONAL MATERIALS SCIENCE
www.elsevier.com/locate/commatsci

Finite element modelling of two phase Fe–Cu polycrystals

Ch. Hartig *, H. Mecking

Department of Materials Science and Technology, Technical University Hamburg-Harburg, Eißendorfer, Str. 42, 21073 Hamburg, Germany

Abstract

The plastic deformation of two-phase iron–copper polycrystals was studied experimentally and modelled by a FEM model calculation, taking into account anisotropic elasticity and crystal plasticity. The two-phase materials in experiment had microstructures ranging between interpenetrating network and matrix/inclusion type and were deformed by compression at room temperature. The measured quantities (macroscopic stress and strain, elastic strains and texture) were compared with the results from the FEM model calculation. The stress vs. strain dependence as obtained from the FEM-model appears to be in good accordance with experimental results. Good predictions of the texture evolution were found in cases only, where local micromechanical interactions are not too much influenced by the heterogeneity of the microstructure. The implications of these results for the development and use of FEM schemes for modelling heterogeneous polycrystal plasticity are discussed.

Keywords: Polycrystal plasticity; Two-phase polycrystals; FEM model; Texture evolution

1. Introduction

Microstructures consisting of two ductile phases occur in many materials of technological interest (α/β-titanium alloys, duplex steels, Ni-base superalloys, Cu–Nb). Thereby, important questions are: How do the properties of the individual crystallites of two phases combine to form the macroscopic properties of the two-phase compound, and how do the individual properties of one phase change due to the presence of the other phase. Answers to these questions are of interest for the processing of materials and for the prediction of the mechanical behaviour of two-phase materials.

This paper mainly focuses on the influence of the microstructure (volume fractions and arrangement of grains of both phases, interfaces) and the distribution of grain orientations in a two-phase

* Corresponding author. Tel.: +49 40 428782276; fax: +49 40 428784070.
E-mail address: hartig@tu-harburg.de (Ch. Hartig).

0927-0256/$ - see front matter © 2004 Elsevier B.V. All rights reserved.
doi:10.1016/j.commatsci.2004.09.030

material which undergoes plastic deformation by dislocation slip.

In order to clarify the influence of arrangement of phases and grains for a wide range of microstructures it is essential to develop models for the description of deformation which can take into account not only the crystallography of slip but also the interaction of neighbouring grains. Following the recommendations on modelling polyphase plasticity given by [1] the complexity of this task should be tackled by a appropriate simulation method (FEM model or self-consistent technique) in combination with a experimental study of a two phase model material. In a previous work [2] experimental results for a model material (Fe–Cu) were compared with calculations done with a viscoplastic self-consistent model [3]. It was found that such a model gives the softer phase a much higher compliance than in reality, i.e. the soft phase (Cu) deforms to such a large extent that the modelled flow stresses of the compound are too low and the modelled texture of the soft phase is much too strong. The present work is aimed at a comparison of experimental results with model calculations after a three dimensional FEM model using single cystal plasticity theory. Meanwhile such models are well developed [4–7], and were used for texture modelling with success in the case of single phase polycrystals [4,5].

2. Experimental

The details concerning the production of polycrystalline iron–copper samples, stress strain testing and determination of texture have been presented in a previous paper [2]. Therefore only a short outline will be given here.

Iron–copper polycrystals were produced from mixtures of iron and copper powder by powder metallurgy. The iron–copper polycrystals had a volume fraction of iron of 0%, 17%, 50%, 83% and 100%. The samples were named after their composition (e.g. Fe17–Cu83 means 17 vol% iron and 83 vol% copper). The microstructures of the two-phase materials (Fig. 1) ranged between inclusion/matrix type (Fe17–Cu83, Fe83–Cu17) and an interpenetrating network of both phases (Fe50–Cu50). The grain size of the homogeneous materials as well as of the single phases in the two-phase polycrystals was 1–15 μm for iron and copper.

Compression tests on cylindrical samples ($h = 9$ mm, $d = 6$ mm) were performed at room temperature with a strain rate $\dot{\varepsilon} = 10^{-4}\ \mathrm{s}^{-1}$. All σ–ε curves were friction corrected assuming the value $\mu = 0.235$ for the coefficient of friction. The stress exponents $n = \partial \ln \dot{\varepsilon} / \partial \ln \sigma$ of single-phase iron and copper were determined experimentally from rate changes in compression tests and used as input parameter for model calculations.

For studies of texture development pole figures were measured with an X-ray goniometer for three reflections of each phase (iron: {200}, {211}, {220}/copper: {200}, {220}, {311}) in middle sections of the compression specimens. Orientation distribution functions (ODF's) and inverse pole figures could be calculated from the measured pole figures for each phase separately using the WIMV-algorithm [8] in the popLA texture package [9].

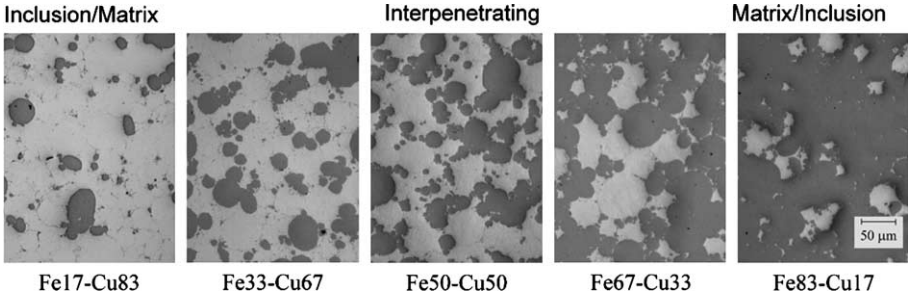

Fig. 1. Microstructures of iron–copper polycrystals. Compositions in vol%.

3. Model calculations

For the constitutive part of the model calculation each grain is considered to be a single crystal and its stress strain behaviour is described by the rate dependent, single crystal plasticity theory presented in Refs. [10,11]. The single crystal theory was implemented in Ref. [10] as a UMAT user subroutine for the finite element program ABAQUS®. The following is a short summary of the theory [10,11]. The material flows via dislocation motion. The total deformation gradient F is given by

$$\boldsymbol{F} = \boldsymbol{F}^{*} \cdot \boldsymbol{F}^{\mathrm{p}} \tag{1}$$

where $\boldsymbol{F}^{\mathrm{p}}$ denotes plastic shear of the material to an intermediate reference configuration in which lattice orientation and spacing are the same as in the original reference configuration, and where $\boldsymbol{F}^{*}$ denotes stretching (by elastic deformation) and rotation of the lattice. The spatial velocity gradient of the plastic shear flow by dislocation slip is given by

$$\dot{\boldsymbol{F}}^{\mathrm{p}} \cdot \boldsymbol{F}^{\mathrm{p}-1} = \sum_{\alpha} \dot{\gamma}^{\alpha} \boldsymbol{s}^{\alpha} \otimes \boldsymbol{m}^{\alpha} \tag{2}$$

where the slip system α is defined by the orthogonal pair of unit vectors $(\boldsymbol{s}^{\alpha}, \boldsymbol{m}^{\alpha})$ and $\dot{\gamma}^{\alpha}$ is the slip rate in this system. The slip direction and slip normal $\boldsymbol{s}^{\alpha,*}$ and $\boldsymbol{m}^{\alpha,*}$ in the deformed configuration are related to the corresponding vectors in the reference configuration by

$$\boldsymbol{s}^{\alpha,*} = \boldsymbol{F}^{*} \cdot \boldsymbol{s}^{\alpha}, \qquad \boldsymbol{m}^{\alpha} = \boldsymbol{F}^{*} \cdot \boldsymbol{m}^{\alpha,*}. \tag{3}$$

The change of the orientation by plastic deformation and the elastic strain can then be obtained from the polar decomposition $\boldsymbol{F}^{*} = \boldsymbol{V} \cdot \boldsymbol{R}$, where $\boldsymbol{R}$ is the lattice rotation and $\boldsymbol{V}$ is the left stretch tensor, describing the elastic strain. The crystallographic slip is assumed to obey the Schmid law

$$\tau^{\alpha} = \boldsymbol{m}^{\alpha,*} \cdot \sigma \cdot \boldsymbol{s}^{\alpha,*} \tag{4}$$

where τ^{α} is the resolved shear stress in slip system α and σ is the Cauchy stress tensor. The stress dependence of the shear rate in that slip system is described by the Norton law

$$\frac{\dot{\gamma}^{\alpha}}{\dot{\gamma}_0} = \mathrm{sgn}(\tau^{\alpha}) \left(\left| \frac{\tau^{\alpha}}{\tau_{\mathrm{c}}^{\alpha}} \right| \right)^{n} \tag{5}$$

where $\tau_{\mathrm{c}}^{\alpha}$ is the critical resolved shear stress, n is the stress exponent and $\dot{\gamma}_0$ is a reference strain rate being equal for all slip systems. The work hardening of each slip system is determined by the evolution equation

$$\dot{\tau}_{\mathrm{c}}^{\alpha} = \theta \cdot \dot{\Gamma} \tag{6}$$

assuming isotropic hardening i.e. to be the same in all slip systems regardless of their individual contribution to the total shear rate $\dot{\Gamma}$ (which is $\dot{\Gamma} = \sum_{\alpha} |\dot{\gamma}_{\alpha}|$). The work hardening rate θ was modified for the present work in the form of a Voce law

$$\theta(\Gamma) = \theta_0 \cdot \left(1 - \frac{\tau_0}{\tau_{\mathrm{s}}} \right) \cdot \exp\left(- \frac{\Gamma \cdot \theta_0}{\tau_{\mathrm{s}}} \right) \tag{7}$$

In this law θ_0 is the extrapolated work hardening rate for zero flow stress and τ_0 and τ_{s} are defined as the critical resolved shear stress at the onset of plastic deformation and the saturation shear stress respectively.

Elasticity is incorporated, as described in [10,11], by Hooke's law for anisotropic media. A complete elastic-plastic rate constitutive law is generated by combining the elastic and plastic constitutive laws using Eqs. (1) and (2).

For the calculation of the stress response to a given deformation process a three-dimensional nonlinear finite-element approach was used. The boundary value problem was solved by the method of representative volume elements (RVE). The displacement fluctuation field was forced to be periodic by equating the values at corresponding points of opposite boundaries of the brick shaped RVE. The nodal displacement vectors $\boldsymbol{u}_K$, $\boldsymbol{u}_{K'}$ of all corresponding nodes K and K' at opposite sides N, $-N$ then fulfil the following relation:

$$\boldsymbol{u}_K^{N} - \boldsymbol{u}_{K'}^{-N} = \boldsymbol{u}_{\mathrm{ref}}^{N} \tag{8}$$

with $\boldsymbol{u}_{\mathrm{ref}}^{N}$ the displacement vector of an appropriately chosen reference node. The compression process needed here was simulated by:

$$\boldsymbol{u}_{\mathrm{ref}}^{Z} = \begin{pmatrix} 0 \\ 0 \\ h - h_0 \end{pmatrix}, \quad u_{\mathrm{ref},y,z}^{X} = u_{\mathrm{ref},x,z}^{Y} = 0 \tag{9}$$

with h being the actual and h_0 the initial height and where the strain rate $\dot{\varepsilon}$ with $\dot{\varepsilon} \cdot t = \varepsilon = \ln h/h_0$ was kept constant.

In the numerical simulation of the compression process the RVE shown in Fig. 2 with 10080 elements of 8-node linear brick type was used. Combining 64–192 elements in one grain, there were initially 126 independent orientations in the RVE. In order to represent the microstructures shown in Fig. 1 as realistic as possible, grains with the properties of iron and copper were connected to clusters of approximately 20 grains. Since each hexahedral element contains eight integration points, all variables of this model calculation (stress, strain, orientation, crystallographic shears) are determined at $10080 * 8 = 80640$ integration points. Continuous distributions of pole densities were calculated from the orientation matrices by a method described in [12]. Macroscopic stress vs. strain curves were obtained from arithmetic mean values of all stress and strain values by averaging over all integration points.

To obtain the unknown parameters θ_0, τ_0 and τ_s for the copper and iron phase, model calculations were performed for RVE's of single phase material of copper and of iron solely. The two sets of the three parameters were obtained from a comparison of the experimental and the computed stress vs. strain curves by a method of trial and error. In all model calculations the fcc slip mode $(\langle 110\rangle,\{111\}) = (\boldsymbol{s}^{\alpha}, \boldsymbol{m}^{\alpha})$ was used for copper, whereas for iron the bcc slip mode with $(\langle 111\rangle,\{110\})$ was assumed.

4. Results and discussion

Fig. 3 shows experimental and simulated stress vs. strain curves for compression tests. As one can see in Fig. 3, single phase iron (Fe100) has an extraordinary high upper yield stress due to its carbon content. With $\sigma_{0.2} \approx 410$ MPa the yield stress of iron is nearly four times higher than that of copper ($\sigma_{0.2} \approx 115$ MPa) and about 75 MPa higher than the stress of copper at a higher plastic strain ($\varepsilon_p = 0.8$).

The curves from the model calculations - shown as symbols at selected strains - fit reasonably well with the experimental curves of the two-phase polycrystals. However, systematic deviations occur in the following cases. At larger strains $\varepsilon_p > 0.3$ the simulated flow stresses for the inclusion type microstructure Fe17–Cu83 are too low, whereas the corresponding flow stresses for the "inverse inclusion type" microstructure Fe83–Cu17 are

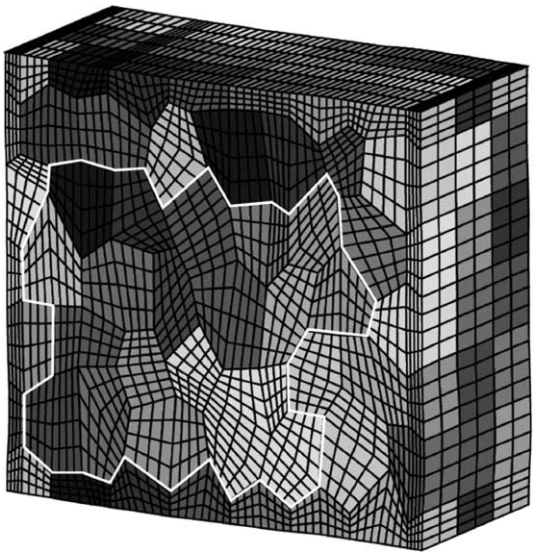

Fig. 2. Representative volume element with 126 grains and 10080 elements. The grains have prismatic shape and are coloured with respect to their orientation. The white border indicates an embedded particle of the second phase.

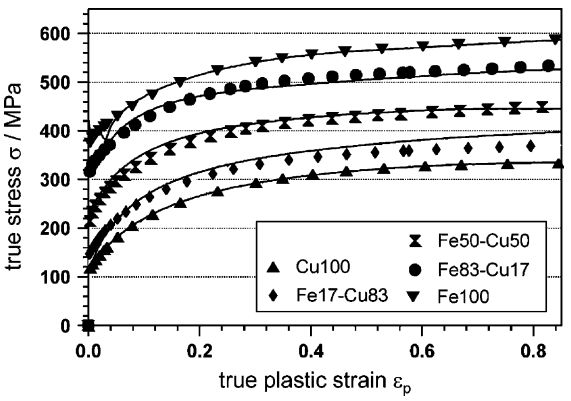

Fig. 3. Stress–strain behaviour of iron–copper polycrystals measured in compression tests at room temperature and constant strain rate (solid lines) in comparison with results from FEM calculations (symbols).

too high. Only for Fe50–Cu50 displaying a microstructure of two interpenetrating phases the simulated stress vs. strain curve is in good accordance with the experimental curve situated nearly in the middle between the single phase materials Fe100 and Cu100. It is also important to note that the experimental observed work hardening in Fe17–Cu83 at strains $\varepsilon_p < 0.08$ is distinctly greater than the corresponding work hardening of the two neighbouring compositions, Cu100 and Fe50–Cu50. Also this hardening effect is not predicted in the simulated stress vs. strain curve of Fe17–Cu83.

The iron phase starts deforming plastically in the model almost simultaneously after the onset of plastic deformation of the copper phase. A modelled macroscopic plastic compression strain of $\varepsilon_p = 0.21\%$ for the Fe17–Cu83 RVE was found to be composed from the two mean strains $\langle\varepsilon_p(\mathrm{Fe})\rangle = 0.07$ and $\langle\varepsilon_p(\mathrm{Cu})\rangle = 0.24$. Even for larger macroscopic strains $\varepsilon_p = 60\%$ the difference between the mean iron and copper strains increases only moderately up to $\langle\varepsilon_p(\mathrm{Cu})\rangle - \langle\varepsilon_p(\mathrm{Fe})\rangle \approx 20\%$. As a consequence the simulated stress vs. strain curves follow quite closely a simple rule of mixtures, i.e. the macroscopic flow stress of the two-phase polycrystal can be calculated as the weighted arithmetic mean of the flow stresses of the two constituent phases at a constant strain. Accordingly the modelled flow stress depends almost linear on the volume fraction. The experimental flow stresses show a weakly sigmoidal behaviour, i.e. for Fe-inclusions in copper the flow stress is higher than for a linear relation, for the interpenetrating microstructure it is equal and for Cu-inclusions in iron the flow stress is lower.

The texture development after compression deformation in both phases of iron–copper polycrystals led to the typical fibre type deformation textures of single phase iron and copper. In the copper phase the ⟨110⟩-fibre component was observed and in the iron phase two fibre components at ⟨001⟩ and ⟨111⟩. From the FEM model calculations of the pure phases the same textures as measured were calculated (see comparison of inverse pole figures in Fig. 4). The accordance between experiment and model calculation for these two cases is very good: Not only the orientation

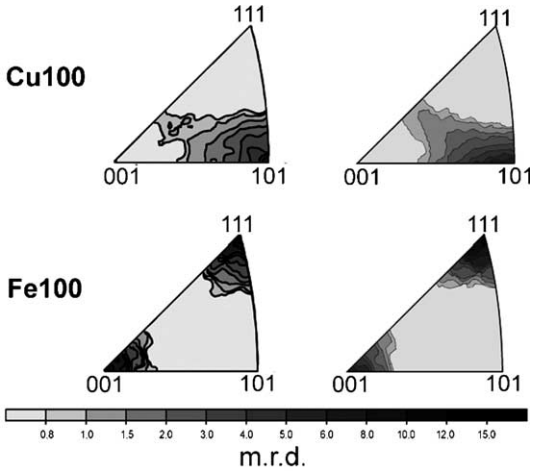

Fig. 4. Inverse pole figures of pure iron and copper after compression with $\varphi = 0.9$ from experiment (left) and FEM model (right). The grey shades are scaled in multiples of a random distribution.

of the fibre components fits very well with the experiment but also their shape and density. This is an improvement in comparison to conventional texture simulation by Taylor or self consistent models, where components develop very strongly resulting in theoretical textures much sharper than experimental textures for a given deformation.

In contrast to this result the theoretical texture development of the two-phase polycrystals is in bad agreement with the experimental textures (Fig. 5). This becomes very obvious in the case of the experimental pole density of the minority copper-phase which weakens and develops irregular maxima for decreasing copper volume fractions. However the modelled pole density of copper remains almost constant with decreasing copper volume fraction (Fig. 5).

For the hard iron phase a moderate decrease of the experimental pole density occurs for decreasing iron volume fractions. This tendency is in qualitative agreement with the modelled texture: The ⟨111⟩- and ⟨100⟩-fibres are spreading along the ⟨001⟩–⟨111⟩-traverse.

The discrepancy between model and experiment for the texture evolution of the soft copper phase may be explained by different reasons:

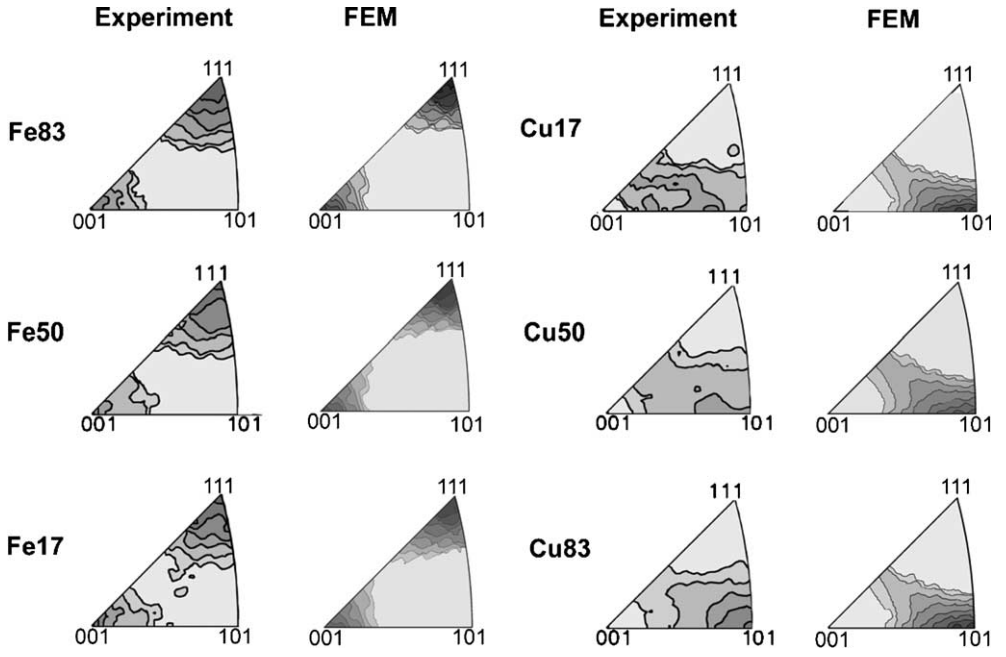

Fig. 5. Inverse pole figures of two-phase iron–copper compounds after compression with $\varphi = 0.9$ from experiment and FEM model.

The soft copper phase has to accommodate large local deviations from the global strain due to local interactions with the harder iron phase. This local interaction which can be quite complicated due to the shape and distribution of neighbouring iron particles should incorporate groups of more than one grain and may not be represented well enough within the scope of the RVE in this model calculation. Also a remeshing procedure may be necessary for a better registration of large inhomogeneous local shears which are necessary for a irregular texture evolution.

Another reason for the insufficient verification of the texture of the copper phase may be due to the local change of the activation of slip systems, which may not occur rapidly enough under the condition of isotropic hardening in the present model calculation.

In order to give a more clear idea about the local stress and strain variations a plot of the typical variation of stresses and strains on a path across the RVE is shown in Fig. 6. It can be clearly recognized that the deformation gradient as well as the stress varies substantially and crystals experience

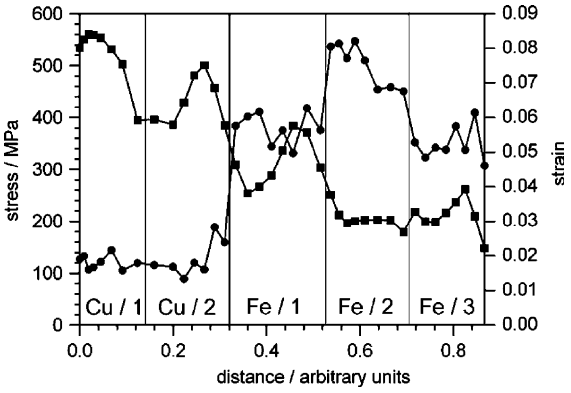

Fig. 6. Compression stresses (●) and strains (■) on a path through the RVE at centres of connected elements after a macroscopic strain of $\varphi = 0.13$. The vertical lines indicate grain and phase boundaries.

local strains that deviate from the nominal value applied to the entire RVE. The deviation of these quantities from the mean is a consequence both of the grain properties (orientation, hardening behaviour, elasticity) and of the interaction with its neighbourhood. Distinct stress and strain

gradients occur in the present case at boundaries between grains of the same phase and at the phase boundary between copper and iron. It can be also recognized from Fig. 6 that the strain variation within each of the phases is of the same order of magnitude as the strain variation between the soft copper and hard iron phase, in accordance with the moderate difference of the mean strains stated above. The local gradients of strain can become quite high, especially at higher macroscopic strains. As a consequence the variation of strains is only restricted to narrow regions in the order of 1–2 elements at the phase boundary. From this result it becomes obvious that large local strain deviations incorporating a group of several grains (i.e. 100–200 elements) seem to be quite seldom. The reason for this behaviour has to be traced to shortcomings of the geometry of the present RVE (arrangement of grains, number of elements per grain) or to the single crystal material law. If the number of elements per grain will give the main improvement for the texture evolution of the soft phase, much more computational effort than in the present work will be required. Also the interface between the soft and hard phase may play a more important role which aspect may be treated by special methods [13]. For the influence of the arrangement of grains, number of grains in the RVE etc. further studies will be conducted in the future.

An indication for a change of material laws in the two phase microstructure can be taken from a comparison of elastic strains in experiment and FEM-model. Fig. 7 shows this comparison for the case of Fe50–Cu50 and macroscopic plastic strains $\varepsilon_p < 2\%$. Similar as for the texture simulation the accordance between experiment and model is better for the hard Fe-phase than for the soft Cu-phase which shows distinctly lower elastic strains (i.e. stresses) in the experiment than in the model. Thus the evolution of stress in the model following the single phase behaviour may be only true for the harder iron phase. A more detailed understanding of the plastic strain hardening of the softer phase may be possible if more experimental information about the partition of plastic strains will be available. Experiments concerning this task will be conducted in the near future giving more evidence and advice for the introduction of a modified material law for the softer Cu-phase.

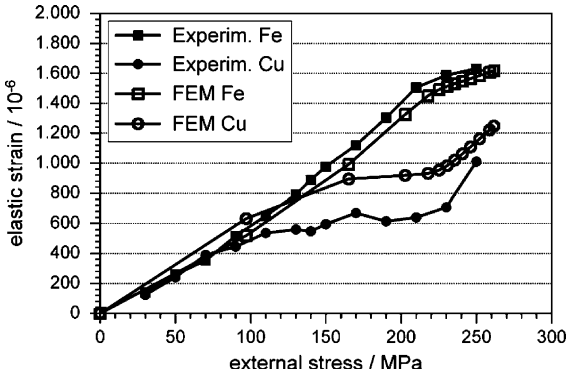

Fig. 7. Mean elastic strains of iron and copper in a Fe50–Cu50 polycrystal as function of the external stress measured by neutron diffraction [14] in comparison with FEM results.

5. Conclusions

This investigation deals with the effects of plastic interaction between a soft phase (i.e. copper) and a hard phase (i.e. iron) in two-phase mixtures of ductile polycrystalline particles. The stress–strain behaviour and the texture evolution under compression was modelled with a crystal plastic FEM model and compared with experimental results. The main conclusions drawn from these comparisons are the following:

1. Both phases start plastic deformation almost simultaneously. Thereby the hard iron phase takes distinctly higher stresses and the copper phase takes higher strains. The difference of the mean strains between iron and copper increases moderately up to large total strains.
2. The calculated stress vs. strain behaviour is in reasonable good agreement with experiment. Deviations occur for the inclusion type microstructures in the sense of a overrepresentation of the minority phase: With iron particles as inclusion the flow stress of the model is higher than in experiment whereas for embedded copper particles it is lower.

3. The texture evolution of the pure phases is in good quantitative agreement with experiment. The texture evolution of the iron phase for the two phase material shows a better agreement between the FEM model and the experiment than the texture evolution of the copper phase. The quality of the texture evolution of the copper phase may be improved by a modified model calculation taking into account more different arrangements of grains or modified material laws.
4. A change of the hardening behaviour of the softer Cu phase and/or plastic strain partition of the two phase material can be concluded from a comparison between measured and modelled elastic strains of the Fe- and Cu-phase.

Acknowledgments

The authors are thankful for the financial support from the German Research Foundation (DFG) for the Collaborative Research Centre 'Micromechanics of Multiphase Materials' (SFB 371, project B1). Dr. M.R. Daymond (Rutherford Appleton Laboratory, England) is kindly thanked for advice and discussions in performing neutron diffraction experiments.

References

[1] Y.J.M. Brechet, P. Dawson, J.D. Embury, C. G'sell, S. Suresh, H.-R. Wenk, Mater. Sci. Eng. A 175 (1994) 1–5.
[2] B. Commentz, Ch. Hartig, H. Mecking, Comput. Mater. Sci. 16 (1999) 237–247.
[3] R.A. Lebensohn, G.R. Canova, Acta Mater. 45 (1997) 3687–3694.
[4] D.P. Mika, P.R. Dawson, Mater. Sci. Eng. A A275 (1998) 62–76.
[5] A. Bertram, T. Böhlke, M. Kraska, in: D.R.J. Owen, E. Oñate, E. Hinton (Eds.), Proceedings of 5th International Conference on Computational Plasticity, Barcelona, Spain, International Center for Numerical Methods in Engineering (CIMNE), 1997, p. 895.
[6] A.J. Beaudoin, H. Mecking, U.F. Kocks, Phil. Mag. A 73 (1996) 1503–1517.
[7] F. Barbe, S. Forest, G. Cailletaud, in: E. Bouchaud, D. Jeulin, C. Prioul, S. Roux (Eds.), Proceedings of the NATO Advanced Study Inst. Physical Aspects of Fracture, Kluwer Academic Publishers, Dordrecht, 2001, pp. 191–206.
[8] S. Matthies, G. Vinel, Phys. Status Solidi B 112 (1982) 111–120.
[9] Preferred orientation package, Los Alamos (popLA), Los Alamos National Lab. LA-CC-89-18, Los Alamos, NM.
[10] Y. Huang, Report Mech-178, 1991, Division of Applied Sciences, Harvard University, Cambridge, MA.
[11] R.J. Asaro, J. Appl. Mech. 50 (1983) 921–934.
[12] S. Matthies, G.W. Vinel, Mat. Sci. Forum 157–162 (1994) 1641–1646.
[13] O. Diard, S. Leclercq, G. Rousselier, G. Cailletaud, Comput. Mater. Sci. 25 (2002) 73–84.
[14] J. Laakmann, M.R. Daymond, H. Mecking, Ch. Hartig, in press.